

Production of Gas Diffusion Layers with Tunable Characteristics

Matthew F. Philips, Gert-Jan M. Gruter,* Marc T. M. Koper, and Klaas Jan P. Schouten

Cite This: *ACS Omega* 2022, 7, 23041–23049

Read Online

ACCESS |



Metrics & More

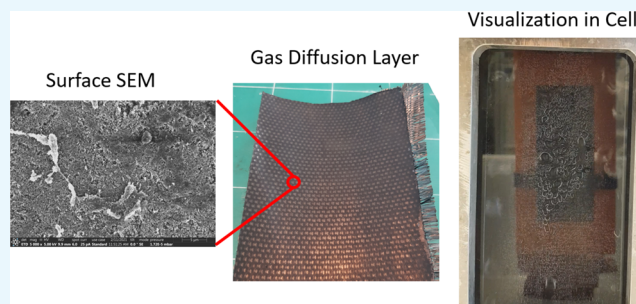


Article Recommendations



Supporting Information

ABSTRACT: Gas diffusion electrodes (GDEs) allow electrochemical reactions to occur at higher rates by enhancing the mass transport of gaseous reactants to the catalyst. These electrodes are made of two layers: the catalyst layer and the gas diffusion layer (GDL). The catalyst layer is frequently studied for gas diffusion electrodes, and the GDL is rarely a focus. Consequently, no studies investigate interaction effects that may be present between these two layers. To study such interactions, it must be possible to obtain GDLs with various characteristics. This study uses a design of experiments to understand how multiple factors in the production method for GDLs can be adjusted to tune the characteristics of the GDL. These GDLs are particularly intended for the electrochemical reduction of CO₂. The conductance through the GDL, surface conductivity, thickness, elasticity, hydrophobicity, and porosity are measured for the 26 synthesized electrodes, and the top influential production factors are identified for each characteristic.



INTRODUCTION

Gas diffusion electrodes (GDEs) have found use in fuel cells, various electrolyzer applications, air batteries, and photocatalytic reactions.^{1–7} Gas diffusion electrodes (GDEs) enhance the mass transfer of gas reactants in electrochemical reactions by creating a three-phase boundary where the gaseous reactant contacts the electrolyte right at the catalyst interface. This enhancement of mass transfer allows for much higher reaction rates to be achieved than in other types of electrochemical technologies (e.g., three-dimensional, 3D electrodes, trickle flow electrodes, etc.). A GDE consists of a gas diffusion layer (GDL) and a catalyst layer. Both layers can affect the overall performance of the GDE.^{3,8–11} Therefore, it is crucial to develop methods to produce GDLs with different characteristics so they can be screened with other catalyst layer factors.

A GDL typically consists of a microporous layer and a macroporous layer. The microporous layer is typically produced with some type of carbon and a hydrophobic binder such as poly(tetrafluoroethylene) (PTFE).¹² Additionally, for wet methods, a solvent is employed. There are a few studies that we are aware of that investigate how different materials used in GDL production can affect a characteristic of the finished GDL. Schulze et al.¹³ found that using more carbon black in the initial powder mixture for their electrodes changed the hydrophobicity of the electrode from hydrophobic to hydrophilic. Kolyagin et al.¹⁴ similarly found that increased PTFE content in the GDL changes the hydrophobicity of the GDL from hydrophilic to hydrophobic. They also found that increasing the PTFE content decreases the structure's surface area and increases the average diameter of hydrophilic pores.

Maja et al.³ studied the effect of the carbon type used in their GDLs on the performance of their GDEs for metal-air batteries. They found that using oil-furnace carbons (Vulcan XC72R and Black Pearls 3700) rather than acetylene black resulted in larger wet pore volumes in their active layer and resulted in poorer electrode stability.

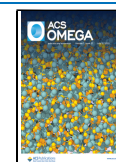
In terms of production process studies, we are only aware of one study that investigates in some detail how the production method for the GDL affects a characteristic of the GDL. Moussallem et al.¹⁵ found that increasing the applied pressure during their production process of GDLs for oxygen depolarized cathodes decreased the structures' porosity. Although these studies link one production factor to one characteristic, many other factors can influence these characteristics, and there are other characteristics of a GDL that can affect the performance of a GDE. Other potential, influential characteristics of GDLs that have been reported in studies include the conductivity and elasticity.^{3,10,11,13,15–25}

The GDL production method from this study was used to produce GDLs in our recent work published on optimizing the CO₂ to formate reaction, where we showed 99% current efficiency at 400 mA/cm² for a 2-h experiment.⁹ These GDLs contain a macroporous layer (woven carbon) and a microporous layer (acetylene black + PTFE) and are generally

Received: December 9, 2021

Accepted: June 7, 2022

Published: June 27, 2022



thicker than traditional GDLs. In this way, the GDL can be used in a configuration where it is directly in between a gas and a liquid phase. This thicker GDL allows higher hydrostatic head pressures to be maintained inside an electrochemical cell and circumvents the need for additional inserts (e.g., percolator) to avoid electrode flooding. Consequently, some of the conclusions from this study may not be valid for thinner GDLs or GDLs produced from a different method.

In this study, GDLs are produced using a wet dough and a hot pressing method similar to the method of Tomantschger et al.¹⁹ We look at 11 factors in our GDL production method and measure six characteristics of the GDL. The goal of this study is to identify which factors in the GDL production method affect each characteristic of the GDL, and we achieve this using a design of experiments (DOE). The results from this study provide a method to produce 26 GDLs with varying characteristics as well as lay the groundwork for future studies to focus on these factors and better explain how these factors are influential to the GDL characteristics.

EXPERIMENTAL SECTION

GDL Synthesis. The synthesis method used for all GDLs was adapted from a method developed earlier in our laboratory.²⁶ Soltex acetylene black 75%-03 carbon (15 g) was weighed and placed in a Bourgini (kitchen) mixer. The appropriate amount of PTFE dispersion 30 (average dispersion particle size of 0.220 μm) was added to 60 mL of a 1:1 volume isopropyl alcohol (IPA)/water mixture and stirred for 1 min. The mixer was turned on at the lowest speed, and the PTFE mixture was slowly added to the mixer. IPA/water (10 mL, 1:1 volume) was used to rinse the beaker containing the initial PTFE mixture and added to the mixer. After 1 min of mixing, a dough-like mixture was collected. The obtained dough was rolled with a marble rolling pin for about 10 min. This allows the material to become more workable to obtain a larger structure.

The dough was then rolled to the desired thickness using a cross-rolling technique. The final dimensions of the rolled doughs were 200 mm \times 125 mm. The dough rectangle was placed on aluminum foil on top of a flat steel compression plate. A paint roller was used to apply PTFE dispersion 30 diluted 50% with 1:1 volume IPA/H₂O to the back of the dough. Carbon fiber fabric (plain weave 3 k) was used as the current collector and placed on top of the dough. Expanded metal mesh was placed on top of the current collector, then another layer of aluminum foil, and then a compression plate. A figure of the order of layers is shown in the Supporting Information (Figure S1). The compression plates were then placed into a Carver heated press (Model number 4533) and pressed in three stages at various temperatures, pressures, and durations according to the DOE matrix. A figure plotting the temperature and pressure profile for GDL 17 is shown in the Supporting Information (Figure S2). GDLs of 10 cm \times 18 cm were cut from the end structure. A picture of what these structures typically look like with the layers labeled is shown in Figure 1. A schematic outlining the layers of the GDL is shown in the Supporting Information (Figure S3)

Design of Experiments. Eleven factors in the production method were considered for a DOE. We acknowledge that other factors can influence the final characteristics of the GDL from this method (e.g., the type of binding agent, carbon type, solvents used, binder particle size, ratio of solvent to water, etc.). However, including additional factors in a DOE would

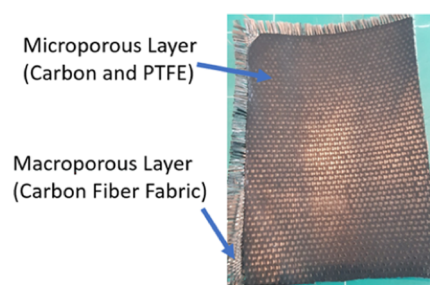


Figure 1. Picture of a GDL produced from the production process studied. Adapted with permission from Philips, M. F.; Pavesi, D.; Wissink, T.; Figueiredo, M. C.; Gruter, G.-J. M.; Koper, M. T. M.; Schouten, K. J. P. Electrochemical CO₂ Reduction on Gas Diffusion Electrodes: Enhanced Selectivity of In–Bi Bimetallic Particles and Catalyst Layer Optimization through a Design of Experiment Approach. Copyright 2022 ACS Applied Energy Materials.

substantially increase the number of experiments required to complete. The factors chosen for this study are the temperature, pressure, and duration of each of the three steps in the pressing process, the PTFE content in the initial dough mixture, and the thickness the dough was rolled to before pressing. The software JMP was used to create a Definitive Screening Design (DSD) of Experiments. This is a small but efficient design used to identify the most influential factors on a response (characteristic) and thus can be used to reduce factors.²⁷ Each production factor was tested at three levels shown in the experimental matrix in Table 1.

Table 1. Levels of Each Production Factor Studied

production factor	low level	center level	high level
PTFE wt %	20	35	50
rolling thickness setting	4 (thinner setting)		2 (thicker setting)
time stage 1 (min)	5	32.5	60
pressure stage 1 (Ton)	0.5	10.25	20
temperature stage 1 (°C)	80	140	200
time stage 2 (min)	5	32.5	60
pressure stage 2 (Ton)	0.5	10.25	20
temperature stage 2 (°C)	280	307.5	335
time stage 3 (min)	5	32.5	60
pressure stage 3 (Ton)	1	13	25
temperature stage 3 (°C)	300	317.5	335

The factors were bounded by initial testing and development of this GDL method. 20 wt % PTFE content was chosen as the lower bound because the dough is more difficult to form with a lower PTFE content. 50 wt % PTFE was selected as the upper bound to try to keep the conductivity of the GDLs as high as possible. The time of each stage varied from 5 to 60 min. These values were chosen to see how short a stage could last to decrease the overall production time. The first stage in the pressing process is designed to evaporate the IPA and H₂O in the structure. This can be done at a slow rate (80 °C) or a fast rate (200 °C). The second stage in the pressing process was designed to decompose surfactant present in the PTFE dispersion and fluidize the PTFE in the structure. The third stage in the process is meant to further facilitate the

fluidization of PTFE in the structure. The pressures of the stage were varied from 0.5 to 25 Ton, with the last stage having a slightly higher range in levels. This was done to observe the effect of higher pressures when the PTFE is more fluid.

The production conditions for each GDL are shown in the Supporting Information (Table S1). Repeats were performed for three electrodes to validate the reproducibility of the method. The analyses of the repeats are shown in the Supporting Information (Figures S4–S18).

Resistance/Conductance Measurements. The surface and through-plane resistance of the GDL will directly affect the full cell potential. Contact resistance was used to measure the surface and through-plane resistance. Copper 101 alloy bars set in a plastic frame were used to make contact on the surfaces of the GDLs, and a PCE Instruments milliohm meter was used for the measurement. The plastic frame and GDLs were placed in a Carver Press AutoFour/3015-PL, H and pressed at a minimum pressure of 0.5 ton for 30 s before recording the resistance. This process was repeated on the opposite end of the GDL. 24.2 cm² of total contact area for through-plane measurements was used. A separation of 1 cm was used for surface resistance measurements. Resistance and resistivity values were converted to conductance and conductivity values for analysis.

Elasticity and Thickness Measurements. The elasticity of the GDL can affect how the GDL bends during its operation inside the cell, which can create nonuniform electrolyte flow over the electrode surface if the GDL is not stiff enough. Additionally, the thickness of the GDL can affect the design specifications for gaskets and the sealing around the GDE inside the cell. For the elasticity, an Instron 5565 tension tester was used to measure the Young's modulus of the GDLs. Six 10 mm × 80 mm samples were cut from the 100 mm × 180 mm structure using a pre-made die. Three samples were cut from one corner, and another three were cut from the opposite corner of the 100 mm × 180 mm structure. A micrometer was used to measure the average thickness of each sample. The gauge length was 34 mm, and the crosshead speed was 5 mm/min.

Water Contact Angle Measurements. Although the hydrophobicity of the GDL is not measured during reacting conditions, this characteristic could still be useful in future developmental work. For example, the binding capabilities of various catalyst application methods could be affected by this characteristic. A microscope optical system with a backlight was used to picture three water droplets on each GDL. The target water droplet volume for each measurement was 50 μL, and photos were taken within 20 s of droplet contact. The Drop Shape Analysis plugin for ImageJ was used to measure the water contact angle from the pictures.²⁸

Hg Porosimetry Measurements. The porosity of the GDL can influence how much gas dissolving area exists between the GDL and catalyst interface. This would directly impact the ability of a GDE to enhance the mass transfer of gaseous reactants. Hg Porosimetry analysis was outsourced to a third-party analytical lab. The sample mass for each measurement was about 0.25 g. The maximum test pressure was 400 MPa, and the increase and decrease speeds were set to 4 and 5 Pa, respectively. The mercury contact angle was 140.0 degrees. Each GDL was analyzed only once, so no data are available for the method's reproducibility.

Workflow for Analysis. After all of the data for each characteristic was collected, the repeat runs were analyzed

using a *t*-test to verify that the repeat and original GDLs were statistically the same. The stepwise platform in JMP was used for each characteristic to fit a model. All factors, interactions, and square terms were considered. Models were generated using the Bayesian Information Criterion (BIC) and Akaike Information Criterion (AIC) as stopping rules to help prevent overfitting.^{29,30} The models generated from both stopping rules for each characteristic are shown in the Supporting Information (Figures S19–S30). The models created were in the form of eq 1

$$y = b_1X_1 + b_2X_2 + b_3X_3 + \dots + b_rX_r \quad (1)$$

where b_n is the model term coefficient and X_n is the factor variable which can be a multiplicative combination of two factors (two-factor interactions) or a squared factor (for modeling curvature). Interactions between two factors indicate that the trend of the response vs one of the interacting factors can change from positive to less positive (or negative to less negative) with a change in the other interacting factor.

The term coefficients indicate the average change in response for every unit increase of the respective term. These coefficients, however, are affected by the scale of the factor (i.e., if one factor is in milli-units and the other is in kilo-units, there would be six orders of magnitude difference between the two predicted coefficients). Consequently, comparing these coefficients can lead to biased conclusions. However, fitting a model to scaled factors (making the range between the factors two and mean equal to zero) results in coefficients that can be equally compared and allows for concluding which factors are affecting the response the most.³¹

The model terms in the selected GDL characteristic models were sorted based on the coefficients of the scaled factors. This shows which terms are influencing the response the greatest.³² Additionally, *t*-tests were performed on the predicted model coefficients to determine with 95% confidence which coefficients were statistically significant. The null hypothesis of the *t*-tests performed is that the term coefficient is zero. *P*-values were calculated for each coefficient, and the null hypothesis was rejected when the *p*-value was less than 0.05 (95% confidence). In other words, when the *p*-value was below the threshold limit, the respective parameter coefficient was concluded with 95% confidence to be nonzero or statistically significant. All model's *R*² values, root mean square errors, coefficient estimates, and *p*-values for the coefficients are shown in the Supporting Information (Figures S19, S21, S23, S25, S27, and S29). Additionally, model profilers help visualize the models generated as they show a snapshot of the models. 2D plots of each model factor vs the GDL characteristic modeled are shown. These model profilers are shown in the Supporting Information (Figures S31–S36). The top four most influential factors (based on the coefficient estimates for scaled factors) for each characteristic are discussed in more detail, even though there may be more than four statistically significant terms in the generated models.

RESULTS AND DISCUSSION

The tabulated GDL characteristic data are shown in the Supporting Information (Table S2).

Conductance through and Surface Conductivity. Higher conductances through the structure and surface conductivities are desirable because they should lead to lower cell potentials and thus lower energy costs. The model

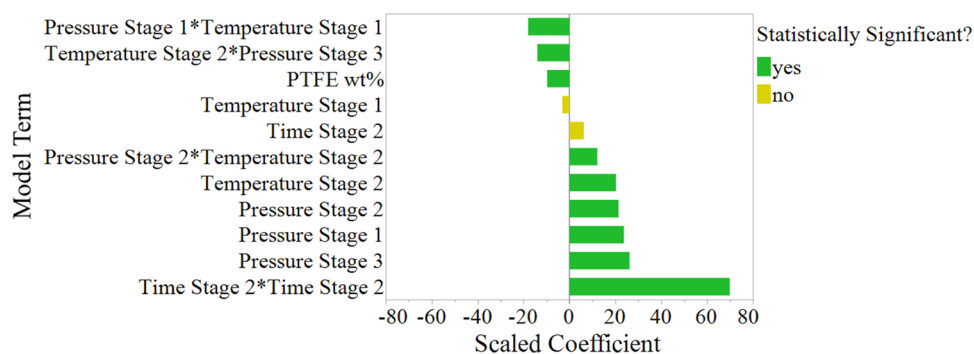


Figure 2. Model term coefficients for scaled factors for the conductance through the GDL. Terms with p -values less than 0.05 are shown as statistically significant.

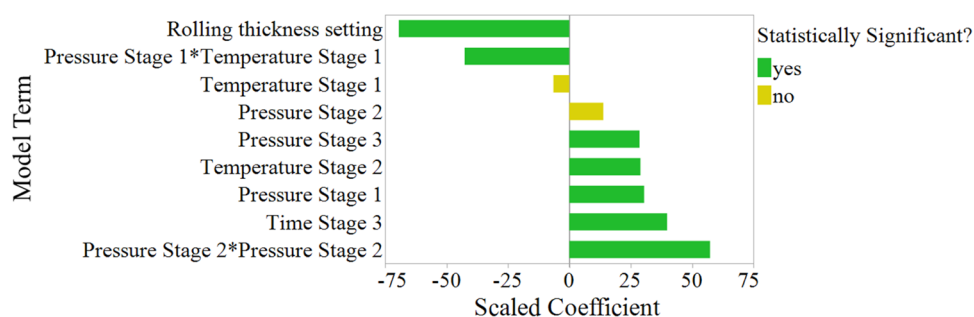


Figure 3. Model term coefficients for scaled factors for the surface conductivity of the GDL. Terms with p -values less than 0.05 are shown as statistically significant.

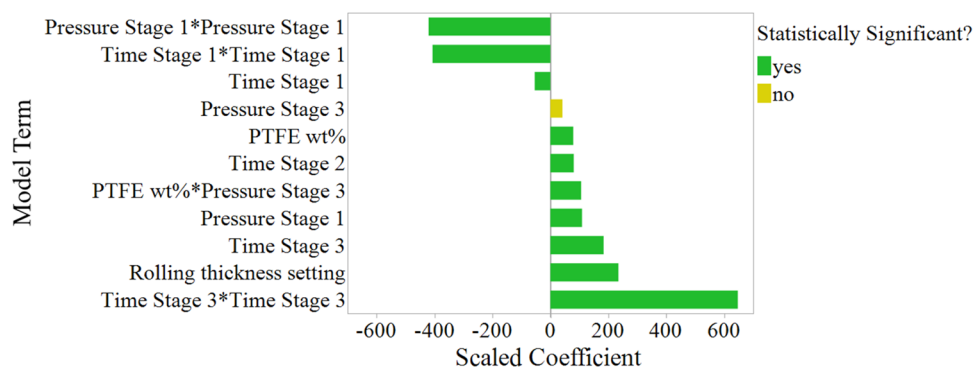


Figure 4. Model term coefficients for scaled factors for the Young's modulus of the GDL. Terms with p -values less than 0.05 are shown as statistically significant.

term coefficients for scaled factors for the conductance through the GDL are shown in Figure 2.

The conductance through the GDL structures is highly affected by the pressures at each stage as well as the time and temperature of the second stage. The coefficient of the squared term of time of the second stage is the largest shown in Figure 2 and therefore affects the conductance through the structure the most. This signifies that there is curvature in the data with respect to the time of the second stage. The pressures at each stage have positive coefficients indicating that increasing pressure increases the conductance through the structure. Additionally, the pressures at each stage show nearly a 2× greater effect on the conductance through the GDL than the PTFE content in the starting mixture.

The model term coefficients for scaled factors for the surface conductivity of the GDL are shown in Figure 3. The surface conductivity is most affected by the thickness of the structure before pressing, the pressure of the second stage, the

interaction between the pressure and temperature of the first stage, and the time of the third stage. The coefficient for the thickness of the structure before pressing is the largest in Figure 3, indicating that this factor affects the surface conductivity of the GDL the most. Similar to the conductance through the GDL, the pressures at each stage have positive coefficients, indicating higher pressures result in higher surface conductivities.

Surprisingly, the pressures at each stage affect the surface conductivity and the conductance through the structure much more than the PTFE content. The positive coefficients for the pressures at each stage (Figures 2 and 3) signify that higher pressures lead to a higher conductance through the structure and a higher surface conductivity. Higher processing pressures can cause an increase in contact between the conductive acetylene black resulting in a higher conducting structure. Additionally, this increased contact between carbon particles can offset the effect of higher PTFE concentrations in the

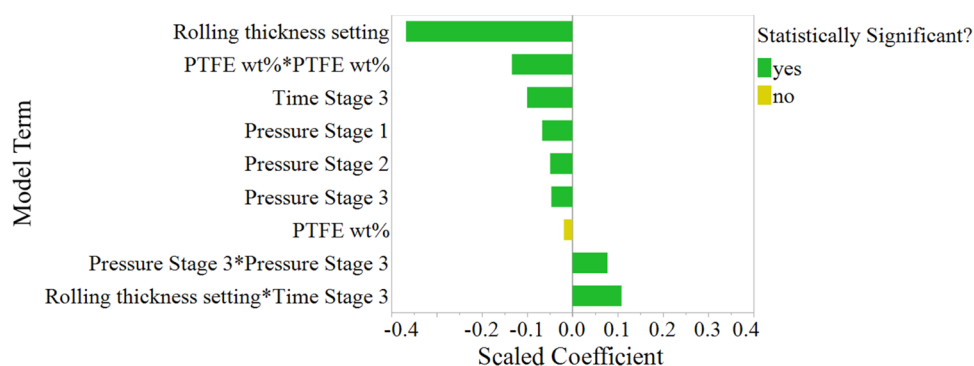


Figure 5. Model term coefficients for scaled factors for the thickness of the GDL. Terms with p -values less than 0.05 are shown as statistically significant.

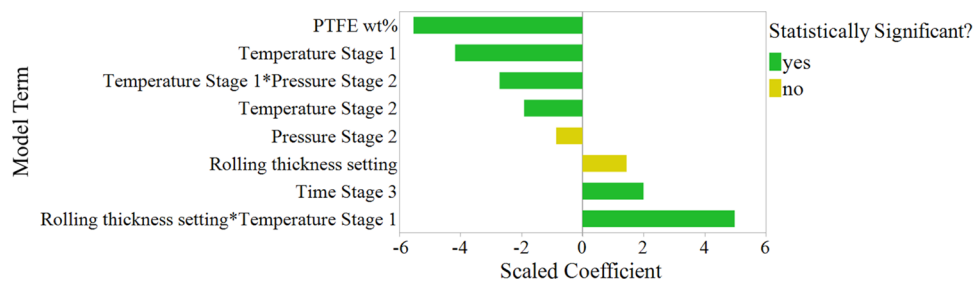


Figure 6. Model term coefficients for scaled factors for the water contact angle of the GDL. Terms with p -values less than 0.05 are shown as statistically significant.

structure, as seen when comparing the conductivities of GDL 3 (low PTFE, low pressures) and GDL 8 (high PTFE, high pressures).

Young's Modulus. Some GDEs can bend outward during operation, touching the membrane and inhibiting electrolyte flow. A higher Young's modulus or stiffer structure is less prone to bending outward during operation. The model term coefficients for scaled factors for the Young's modulus of the GDL are shown in Figure 4.

The Young's Modulus of the GDL structures is highly influenced by the final and initial stage times, the pressure of the first stage, and the thickness of the structure before pressing. The time and pressure of the first stage and the time of the third stage show the highest scaled coefficients for their squared terms, indicating they affect the Young's modulus of the GDL the most and that there is curvature in the data with respect to these factors. Maximum Young's modulus values are predicted near central values for the time and pressure of the first stage, while a minimum value is predicted near the center point for the time of the third stage. These results show that there are higher-order terms at play in influencing the stiffness of the GDL. More experiments are necessary to understand these higher-order relationships better. Nevertheless, the factor space for these experiments has been significantly narrowed down.

Structure Thickness. The model term coefficients for scaled factors for the thickness of the GDL are shown in Figure 5. As expected, the thickness of the dough before pressing influences the final structure's thickness the most out of all of the factors. The PTFE content is the second most influential factor for the final structure thickness. Additionally, as expected, the pressures of each stage have a negative correlation with the thickness of the structure, indicating that as pressure increases, the structure becomes thinner.

The interaction between rolling thickness and time of the third stage shows that a thinner structure is achieved at longer times of the third stage only when the rolling thickness of the dough is set at 2 (thicker). However, when the rolling thickness of the dough is set at 4 (thinner), the time of the third stage is not predicted to affect the thickness of the structure (see Supporting Information Figure S34). The significance of this interaction is most likely explained by the difference in the amount of material between the two rolling thickness settings (e.g., the setting of 2 (thicker) will have more material in the press than a dough with a thickness setting of 4). More material can result in more time required to press the structure to become thinner. Additionally, higher pressures at all stages lead to thinner structures, as seen by their negative coefficients in Figure 5. However, this negative trend for the pressure at the third stage disappears at pressures greater than 10 Ton, as seen in the model profiler (Figure S34).

Water Contact Angle. The hydrophobicity of the GDL directly impacts how the GDE maintains a three-phase boundary. The greater the hydrophobicity of the GDL, the less likely it should be to flood and lose activity.³ The model term coefficients for scaled factors for the water contact angle of the GDL are shown in Figure 6.

The water contact angle, or hydrophobicity, of the GDL structures is highly influenced by the PTFE content in the structure, the temperature of the first stage, and its interaction with the rolling thickness and the pressure of the second stage. The model profiler in the Supporting Information (Figure S35) shows the behavior of these two interactions.

Unexpectedly, the PTFE content is negatively correlated with the hydrophobicity of the structure, suggesting that the more PTFE in the structure, the less hydrophobic it becomes. Analysis of the contact angle of PTFE and the acetylene black

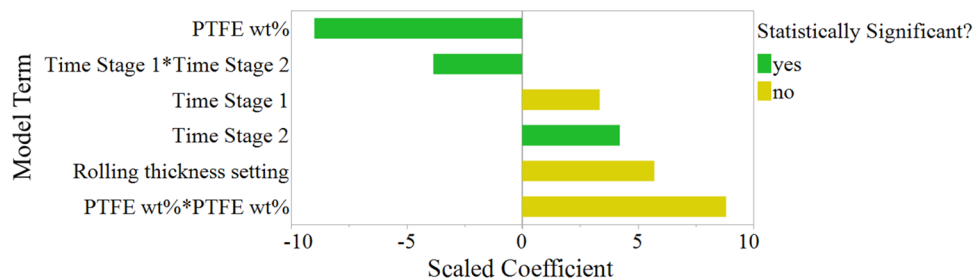


Figure 7. Model term coefficients for scaled factors for the porosity of the GDL. Terms with p -values less than 0.05 are shown as statistically significant.

Table 2. Top Four Influential Factors in the GDL Production Method for Each Characteristic Studied

	Conductance (S)	Surface Conductivity (S/m)	Young's Modulus	Thickness (mm)	Water Contact Angle	Porosity (%)
PTFE content						
Rolling Thickness						
Pressure Stage 1						
Temperature Stage 1						
Time Stage 1						
Pressure Stage 2						
Temperature Stage 2						
Time Stage 2						
Pressure Stage 3						
Temperature Stage 3						
Time Stage 3						

was performed to investigate this trend further. The PTFE had a contact angle of 108° , which agrees with other reported experiments.^{33–35} The water contact angle of acetylene black was measured to be 145° which shows that it is even more hydrophobic than PTFE. Furthermore, this trend with PTFE could be a result of changes in the surface roughness from varying porosities and pore sizes of the GDL. This ultra-hydrophobicity phenomenon is known to occur with rough hydrophobic surfaces.^{36–38} The fact that the water contact angle appears to have a slight positive correlation with the structure's porosity (higher porosities also tend to have higher water contact angles) further supports this idea. Future work should strongly consider and measure the surface roughness of GDLs to identify if there is a correlation between the roughness and hydrophobicity of the layer.

Porosity. The porosity of the GDL will impact the gas dissolving sites and thus the mass transfer of the GDE. A more porous structure should lead to better mass transfer of gaseous

reactant to the reacting sites of the GDE.³⁹ The model term coefficients for scaled factors for the porosity of the GDL are shown in Figure 7.

The PTFE content of the GDL, the times of stages 1 and 2, and the thickness of the structure before pressing affect the porosity of the GDL. The model profiler in the Supporting Information (Figure S36) shows a negative correlation between the PTFE concentration and the porosity of the GDL. This correlation disappears at concentrations above 35 wt %.

The thickness of the structures before pressing is the second largest factor affecting the structure's porosity. The model profiler shows the thinner starting structures (setting 4) tend to lead to GDLs that are more porous. Additionally, the first and second stages' times and their interaction affect the GDL's porosity. At low times of stage one, increasing the time of stage 2 increases the porosity of the GDL. However, at high times of stage 1, increasing the time of stage 2 no longer has a large

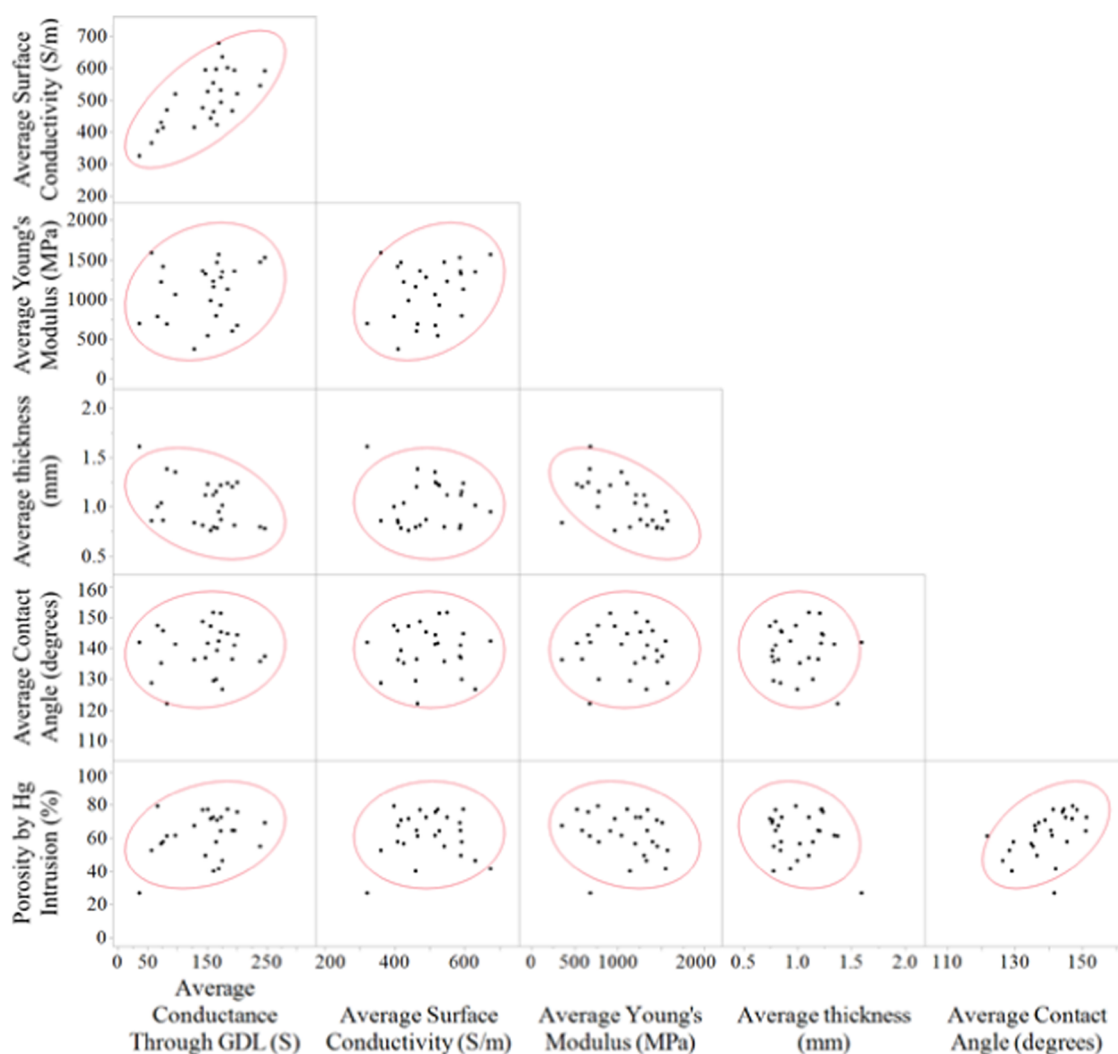


Figure 8. Scatterplot matrix of GDL characteristics.

effect on the porosity (see Figure S36). The significance of the initial structure thickness, the times of the first two stages, and the interaction suggests that solvent evaporation is crucial to creating a more porous structure.

Combined Characteristic Analysis. Table 2 summarizes the top four influential factors for each characteristic. Additionally, we explore if any of the characteristics measured are correlated with each other through a scatterplot matrix shown in Figure 8. Overall, the temperatures of the second and third stages do not significantly impact any of the characteristics studied, as seen in Table 2. Additionally, the pressure of the third stage only affects two characteristics: the conductance through the GDL and the thickness of the final structure. Therefore, it could be possible to combine the second and third stages of this production process since the pressure of the third stage has the same (positive) correlation as the pressure of the second stage for the conductance through the GDL and the pressure of the second stage does not have a large effect on the thickness of the structure.

The density ellipses shown in Figure 8 help emphasize the characteristics that are slightly correlated with each other. The less circular (more elliptical) the red outline is, the more correlated the characteristics are with each other. A few characteristics appear to be slightly correlated with each other,

showing some limitations in the tunability of the GDLs produced from this method. The conductance through the GDL and Young's Modulus appears to be correlated with the structure's thickness. Additionally, there appears to be a slight correlation between the porosity and water contact angle of the GDL as well as the surface conductivity and conductance through the GDL. The correlation between surface conductivity and conductance through the structure is expected since each GDL should have the same skeletal structure of PTFE and carbon. Thus, as the conductance through the structure increases, so should the surface conductivity of the structure. As previously stated, the correlation between the porosity and contact angle of the GDLs can be explained by several studies that show rough surfaces lead to increased hydrophobicity.^{36–38} Hence, the more porous structures likely also have rougher surfaces from the pores resulting in higher water contact angles.

CONCLUSIONS

The most influential factors in the GDL production process for six characteristics have been identified. However, not all of these characteristics appear to be completely independent of each other, and therefore there may be some limitations on the tunability of these structures. The porosity of the GDL and the

hydrophobicity do not appear to be completely independent characteristics, and neither do the surface conductivity and the conductance through the GDL.

Additionally, not all production factors appear to be highly influential in the characteristics of the GDL. The temperature of the third and second stages does not play a prominent role in influencing the characteristics of the GDL. It should be possible to tune GDLs using a method with a combined second and third stage, thus saving time and energy. The results from this study lay the groundwork for future studies to focus on these significant factors and better explain how they may be influencing the various characteristics. Work could be performed to understand better how the factors identified in this study affect the Young's modulus as it is not very clear why these factors are influential. Additionally, future research could investigate if the production method could be reduced to only two stages.

Finally, this study provides a method to produce 26 GDLs with varying characteristics. These results can be used in future studies to investigate the impact of a GDL on the performance of a catalyzed GDE. This also allows for the interaction effects between the GDL and the catalyst layer to be studied, as we have shown in our recent work.⁹ Future research on electrochemical reactions using GDEs can use these recipes to test GDLs with different characteristics and quantitatively understand what makes an ideal GDL.

■ ASSOCIATED CONTENT

SI Supporting Information

The Supporting Information is available free of charge at <https://pubs.acs.org/doi/10.1021/acsomega.1c06977>.

Preparation of GDL; repeat experiments; comparison of models considered for the six characteristics; model profilers for each selected model; and tabulated data (PDF)

■ AUTHOR INFORMATION

Corresponding Author

Gert-Jan M. Gruter – *Avantium, 1098 XH Amsterdam, The Netherlands; Van 't Hoff Institute for Molecular Sciences, University of Amsterdam, 1090 GD Amsterdam, The Netherlands;* orcid.org/0000-0003-4213-0025;
Email: G.J.M.Gruter@uva.nl

Authors

Matthew F. Philips – *Avantium, 1098 XH Amsterdam, The Netherlands; Leiden Institute of Chemistry, Leiden University, 2333 CC Leiden, The Netherlands;* orcid.org/0000-0003-2767-2117

Marc T. M. Koper – *Leiden Institute of Chemistry, Leiden University, 2333 CC Leiden, The Netherlands;* orcid.org/0000-0001-6777-4594

Klaas Jan P. Schouten – *Avantium, 1098 XH Amsterdam, The Netherlands; Present Address: Teijin Aramid BV, Tivolilaan 50, 6824 BW Arnhem, The Netherlands;* orcid.org/0000-0003-4792-0085

Complete contact information is available at: <https://pubs.acs.org/10.1021/acsomega.1c06977>

Author Contributions

The manuscript was written through contributions of all authors. All authors have given approval to the final version of the manuscript.

Notes

The authors declare no competing financial interest.

■ ACKNOWLEDGMENTS

This work was supported by the European Commission under contract 722614 (Innovative training network Elcorel)

■ ABBREVIATIONS

GDE, gas diffusion electrode; GDL, gas diffusion layer; DOE, design of experiments; BIC, Bayesian Information Criterion; AIC, Akaike Information Criterion

■ REFERENCES

- (1) Kolyagin, G. A.; Vasil'eva, I. S.; Kornienko, V. L. Effect of the Composition of Gas-Diffusion Carbon Black Electrodes on Electro-synthesis of Hydrogen Peroxide from Atmospheric Oxygen. *Russ. J. Appl. Chem.* **2008**, *81*, 983–987.
- (2) Monteiro, M. C. O.; Philips, M. F.; Schouten, K. J. P.; Koper, M. T. M. Efficiency and Selectivity of CO₂ Reduction to CO on Gold Gas Diffusion Electrodes in Acidic Media. *Nat. Commun.* **2021**, *12*, No. 4943.
- (3) Maja, M.; Orecchia, C.; Strano, M.; Tosco, P.; Vanni, M. Effect of Structure of the Electrical Performance of Gas Diffusion Electrodes for Metal Air Batteries. *Electrochim. Acta* **2000**, *46*, 423–432.
- (4) Wang, P.; Zhao, J.; Shi, R.; Zhang, X.; Guo, X.; Dai, Q.; Zhang, T. Efficient Photocatalytic Aerobic Oxidation of Bisphenol A via Gas-Liquid-Solid Triphase Interfaces. *Mater. Today Energy* **2022**, *23*, No. 100908.
- (5) Shi, R.; Guo, J.; Zhang, X.; Waterhouse, G. I. N.; Han, Z.; Zhao, Y.; Shang, L.; Zhou, C.; Jiang, L.; Zhang, T. Efficient Wettability-Controlled Electroreduction of CO₂ to CO at Au/C Interfaces. *Nat. Commun.* **2020**, *11*, No. 3028.
- (6) Shi, R.; Wang, Z.; Zhao, Y.; Waterhouse, G. I. N.; Li, Z.; Zhang, B.; Sun, Z.; Xia, C.; Wang, H.; Zhang, T. Room-Temperature Electrochemical Acetylene Reduction to Ethylene with High Conversion and Selectivity. *Nat. Catal.* **2021**, *4*, 565–574.
- (7) Huang, H.; Shi, R.; Zhang, X.; Zhao, J.; Su, C.; Zhang, T. Photothermal-Assisted Triphase Photocatalysis Over a Multifunctional Bilayer Paper. *Angew. Chem., Int. Ed.* **2021**, *60*, 22963–22969.
- (8) Philips, M. F.; Gruter, G.-J. M.; Koper, M. T. M.; Schouten, K. J. P. Optimizing the Electrochemical Reduction of CO₂ to Formate: A State-of-the-Art Analysis. *ACS Sustainable Chem. Eng.* **2020**, *8*, No. 15430.
- (9) Philips, M. F.; Pavesi, D.; Wissink, T.; Figueiredo, M. C.; Gruter, G.-J. M.; Koper, M. T. M.; Schouten, K. J. P. Electrochemical CO₂ Reduction on Gas Diffusion Electrodes: Enhanced Selectivity of In-Bi Bimetallic Particles and Catalyst Layer Optimization through a Design of Experiment Approach. *ACS Appl. Energy Mater.* **2022**, *5*, 1720–1730.
- (10) Uchida, M.; Fukuoka, Y.; Sugawara, Y.; et al. Effects of Microstructure of Carbon Support in the Catalyst Layer on the Performance of Polymer-Electrolyte Fuel Cells. *J. Electrochem. Soc.* **1996**, *143*, No. 2245.
- (11) Kong, C. S.; Kim, D.-Y.; Lee, H.-K.; Shul, Y.-G.; Lee, T.-H. Influence of Pore-Size Distribution of Diffusion Layer on Mass-Transport Problems of Proton Exchange Membrane Fuel Cells. *J. Power Sources* **2002**, *108*, 185–191.
- (12) Philips, M. F.; Gruter, G.-J. M.; Koper, M. T. M.; Schouten, K. J. P. Optimizing the Electrochemical Reduction of CO₂ to Formate: A State-of-the-Art Analysis. *ACS Sustainable Chem. Eng.* **2020**, *8*, 15430–15444.

- (13) Schulze, M.; Lorenz, M.; Kaz, T. XPS Study of Electrodes Formed from a Mixture of Carbon Black and PTFE Powder. *Surf. Interface Anal.* **2002**, *34*, 646–651.
- (14) Kolyagin, G. A.; Kornienko, V. L. New Accelerated Method of Impregnation by Aqueous Electrolyte of Carbon Black Gas-Diffusion Electrodes to Study Their Structural and Electrochemical Characteristics. *Russ. J. Electrochem.* **2011**, *47*, 1268–1273.
- (15) Moussallem, I.; Pinnow, S.; Wagner, N.; Turek, T. Development of High-Performance Silver-Based Gas-Diffusion Electrodes for Chlor-Alkali Electrolysis with Oxygen Depolarized Cathodes. *Chem. Eng. Process.* **2012**, *52*, 125–131.
- (16) Li, A.; Wang, H.; Han, J.; Liu, L. Preparation of a Pb Loaded Gas Diffusion Electrode and Its Application to CO₂ Electroreduction. *Front. Chem. Sci. Eng.* **2012**, *6*, 381–388.
- (17) Del Castillo, A.; Alvarez-Guerra, M.; Solla-Gullón, J.; Sáez, A.; Montiel, V.; Irabien, A. Sn Nanoparticles on Gas Diffusion Electrodes: Synthesis, Characterization and Use for Continuous CO₂ Electroreduction to Formate. *J. CO₂ Util.* **2017**, *18*, 222–228.
- (18) Pozio, A.; Cemmi, A.; Carewska, M.; Paoletti, C.; Zaza, F. Characterization of Gas Diffusion Electrodes for Polymer Electrolyte Fuel Cells. *J. Fuel Cell Sci. Technol.* **2010**, *7*, No. 041003.
- (19) Tomantschger, K.; Kordesch, K. V. Structural Analysis of Alkaline Fuel Cell Electrodes and Electrode Materials. *J. Power Sources* **1989**, *25*, 195–214.
- (20) Kenjo, T.; Kawatsu, K. Current-Limiting Factors and the Location of the Reaction Area in PTFE-Bonded Double-Layered Oxygen Electrodes. *Electrochim. Acta* **1985**, *30*, 229–233.
- (21) Lasia, A. Impedance of Porous Electrodes. In *ECS Transactions*; ECS, 2008; pp 1–18.
- (22) Lee, H.-K.; Park, J.-H.; Kim, D.-Y.; Lee, T.-H. A Study on the Characteristics of the Diffusion Layer Thickness and Porosity of the PEMFC. *J. Power Sources* **2004**, *131*, 200–206.
- (23) Tseng, C.-J.; Lo, S.-K. Effects of Microstructure Characteristics of Gas Diffusion Layer and Microporous Layer on the Performance of PEMFC. *Energy Convers. Manage.* **2010**, *51*, 677–684.
- (24) Gülzow, E.; Schulze, M. Long-Term Operation of AFC Electrodes with CO₂ Containing Gases. *J. Power Sources* **2004**, *127*, 243–251.
- (25) Gullá, A. F.; Krasovic, J. L. Gas-Diffusion Electrode. WO Patent WO2013/037902 A22013.
- (26) Philips, M. F.; Ansovini, D.; Figueiredo, M. C. C.; Krasovic, J. Method for the Preparation of a Gas Diffusion Layer and a Gas Diffusion Layer Obtained or Obtainable by Such Method. WO Patent WO2020165074A12020.
- (27) *JMP 14 Design of Experiments Guide*; SAS Institute Inc: Cary, NC, 2018.
- (28) Stalder, A. F.; Kulik, G.; Sage, D.; Barbieri, L.; Hoffmann, P. A Snake-Based Approach to Accurate Determination of Both Contact Points and Contact Angles. *Colloids Surf., A* **2006**, *286*, 92–103.
- (29) Claeskens, G.; Hjort, N. L. *Model Selection and Model Averaging*; Cambridge Books, 2006.
- (30) Klimberg, R.; McCullough, B. D. *Fundamentals of Predictive Analytics with JMP*; SAS Institute: Cary, NC, 2013.
- (31) *JMP 14 Fitting Linear Models*; SAS Institute Inc.: Cary, NC, 2018.
- (32) Thompson, J. *Design and Analysis in Chemical Research*, Tranter, R. L., Eds.; John Wiley & Sons, 2000; pp 85–110.
- (33) Włoch, J.; Terzyk, A. P.; Wiśniewski, M.; Kowalczyk, P. Nanoscale Water Contact Angle on Polytetrafluoroethylene Surfaces Characterized by Molecular Dynamics–Atomic Force Microscopy Imaging. *Langmuir* **2018**, *34*, 4526–4534.
- (34) Fox, H.; Zisman, W. The Spreading of Liquids on Low Energy Surfaces. I. Polytetrafluoroethylene. *J. Colloid Sci.* **1950**, *5*, 514–531.
- (35) Ellison, A. H.; Fox, H. W.; Zisman, W. A. Wetting of Fluorinated Solids by Hydrogen-Bonding Liquids. *J. Phys. Chem. A* **1953**, *57*, 622–627.
- (36) Extrand, C. W. Designing for Optimum Liquid Repellency. *Langmuir* **2006**, *22*, 1711–1714.
- (37) Quéré, D. Wetting and Roughness. *Annu. Rev. Mater. Res.* **2008**, *38*, 71–99.
- (38) Marmur, A. From Hydrophilic to Superhydrophobic: Theoretical Conditions for Making High-Contact-Angle Surfaces from Low-Contact-Angle Materials. *Langmuir* **2008**, *24*, 7573–7579.
- (39) Motoo, S.; Watanabe, M.; Furuya, N. Gas Diffusion Electrode of High Performance. *J. Electroanal. Chem. Interfacial Electrochem.* **1984**, *160*, 351–357.